

Numerical experiments on the drift wave–zonal flow paradigm for nonlinear saturation

Cite as: Phys. Plasmas **15**, 122503 (2008); <https://doi.org/10.1063/1.3033206>

Submitted: 28 July 2008 • Accepted: 29 October 2008 • Published Online: 10 December 2008

R. E. Waltz and C. Holland



View Online



Export Citation

ARTICLES YOU MAY BE INTERESTED IN

[Comparisons and physics basis of tokamak transport models and turbulence simulations](#)


Physics of Plasmas **7**, 969 (2000); <https://doi.org/10.1063/1.873896>

[Electron temperature gradient driven turbulence](#)

Physics of Plasmas **7**, 1904 (2000); <https://doi.org/10.1063/1.874014>

[Excitation of zonal flow by drift waves in toroidal plasmas](#)

Physics of Plasmas **7**, 3129 (2000); <https://doi.org/10.1063/1.874222>



Physics of Plasmas Physics of Fluids

Special Topic: Turbulence in Plasmas and Fluids

Submit Today!

Numerical experiments on the drift wave–zonal flow paradigm for nonlinear saturation

R. E. Waltz^{1,a)} and C. Holland²

¹General Atomics, P.O. Box 85608, San Diego, California 92186-5608, USA

²University of California-San Diego, La Jolla, California 92093, USA

(Received 28 July 2008; accepted 29 October 2008; published online 10 December 2008)

This paper confirms that $E \times B$ shearing from toroidally symmetric (toroidal mode number $n=0$) “radial modes” provides the dominant nonlinear saturation mechanism for drift wave ($n \neq 0$) turbulence, which in turn nonlinearly drives the modes. In common usage, this is loosely referred to as the “drift wave–zonal flow paradigm” for nonlinear saturation despite the fact that radial modes have several components distinguished in this paper: a residual or zero mean frequency “zonal flow” part and an oscillatory “geodesic acoustic mode” (GAM) part. Linearly, the zonal flows (and GAMs) are weakly damped only by ion-ion collisions, while the GAMs are strongly Landau damped only at low safety factor q . At high q the Hinton–Rosenbluth residual flow from an impulse vanishes and only the weakly damped GAMs remain. With the linear physics and driving rates of the finite- n transport modes unchanged, this paper argues that GAMs are only somewhat less effective than the residual zonal flows in providing the nonlinear saturation, and in some cases $E \times B$ shearing from GAMs (or at least the GAM physics) appears to dominate: transport appears to be nearly linear in the GAM frequency. By deleting the drift wave–drift wave nonlinear coupling, it is found that drift wave–radial mode *nonlinear coupling triads* account for most of the nonlinear saturation. Furthermore, the $E \times B$ shear components of the radial modes nonlinearly stabilize the finite- n modes, while the diamagnetic components nonlinearly destabilize them. Finally, from wave number spectral contour plots of the time average nonlinear entropy transfer function (and rates), it is shown that the peak in entropy generation coincides with the peak in transport production, while entropy dissipation (like Landau damping) is spread equally over all n modes (including $n=0$). Most of these conclusions appear to hold about equally well for all types of drift wave turbulence. © 2008 American Institute of Physics. [DOI: 10.1063/1.3033206]

I. INTRODUCTION AND SUMMARY OF CONCLUSIONS

The ion temperature gradient–adiabatic electron (ITG-ae) gyro-Landau-fluid simulations of the early 1990s^{1,2} established that the $E \times B$ shear from toroidally symmetric (toroidal mode number $n=0$) “radial modes” provides the dominant nonlinear saturation mechanism for drift wave turbulence. In common usage, this is often loosely referred to as the “drift wave–zonal flow paradigm” for nonlinear saturation (see Ref. 3 for a review). However, more precisely, as this paper emphasizes, the radial modes (labeled by a radial wave number $k_x \neq 0$) actually have several distinguishable components: a residual or zero mean frequency “zonal flow” part and an oscillatory “geodesic acoustic mode” (GAM) part. The $E \times B$ residual flow component is nearly in balance with the ion pressure diamagnetic flow component;^{4,5} hence, radial modes (particularly the zonal flow component) have little net mass flow. As observed in both simulations and experiments, the time average residual (zero mean frequency) of both flows result in equilibrium “profile corrugations” in the equilibrium plasma gradients and $E \times B$ shear near low order rational surfaces.⁵ At experimentally relevant collisionality, zonal flows are weakly damped linearly only by ion-ion collisions (which we ignore) and the GAMs are strongly Landau damped only at low to moderate safety factor q (typical of the core). At high q (typical of the edge) the

Hinton–Rosenbluth residual flow (from an impulse) vanishes and only the slightly damped GAMs remain.^{6,7} GAMs are easily identified in simulations and similarly from experimental diagnostics [like beam emission spectroscopy (BES)] at the tokamak edge by their high frequency.^{8–10} It is more difficult to identify the zero mean frequency peak of the zonal flows with BES, but Fig. 4 in Ref. 10 appears to illustrate a reduction in zonal flows and increase in GAMs by sampling closer to the edge.

The present paper addresses three basic questions: (1) At fixed drift wave linear driving rate, what is the difference between the transport levels from residual zonal flow dominated saturation at the low q (core) and from GAM dominated saturation at the high q (edge) and how is the physics of the radial mode components to be distinguished? (2) What are the main elements of the nonlinear coupling mechanism and which dominate? (3) Does the “paradigm” historically developed from ITG-ae simulations apply equally well to trapped electron mode (TEM), mixed ITG/TEM, and electron temperature gradient–adiabatic ion (ETG-ai) turbulence?

To explore these and other questions, we have done “numerical experiments” with GYRO¹¹ by (a) modifying the linear physics of the radial modes (in Sec. II), or (b) modifying components of the nonlinear coupling convolution (Sec. III). In both modifications, *the linear physics of the finite- n modes is unchanged*. In (a) we increase the q value in the radial

^{a)}Electronic mail: waltz@fusion.gat.com.

modes to trade off the zonal flows in favor of the GAMs, and decrease the $1/R$ curvature in the radial modes to slow down the GAMs and decrease their damping. In (b) we delete various components of the nonlinear coupling to show that drift wave–radial mode coupling dominates.

We find in Sec. II (1) transport increases somewhat as the zonal flow residuals and GAM damping is decreased, but in general $E \times B$ shearing from GAMs *can be* as effective as zonal flows and sometimes appear to dominate zonal flows in limiting the transport; (2) when the GAMs dominate, transport decreases as the GAM frequency is slowed or the GAM damping rate is decreased. We find in Sec. III (3) the drift wave–radial mode $[n=n_1+n_2, n_{1(2)} \neq 0, n_{2(1)}=0]$ triads account for most of the nonlinear saturation although the remaining triads cannot be neglected to get the physical spectrum; (4) coupling to the $E \times B$ shear ($\delta\phi$ –) components of the radial modes nonlinearly stabilize finite- n modes (drift waves), while (5) coupling to the diamagnetic (δf –) components appears to nonlinearly destabilize them.

From $[k_x, k_y]$ spectral contour plots of the time average nonlinear entropy transfer function $[T(\vec{k}) = -2\gamma_k^S S(\vec{k})]$ with $\Sigma_k T(\vec{k}) = 0$, and transfer rate $(2\gamma_k^S)$, we find in Sec. IV that (6) the peak entropy $S(\vec{k})$ generation coincides with peak transport producing modes while entropy dissipation (from Landau damping and more importantly from the high- k_x dissipation) is spread equally over all mode numbers n ($k_y = nq/r$) (including the $n=0$ radial modes). We also find that (7) the transport is unchanged without linear GAM Landau damping which dominates the low- k_x entropy dissipation of the $n=0$ radial modes; and that (8) the (properly normalized) $E \times B$ shearing rate $\hat{\gamma}_E(\vec{k}) = \hat{k}_x^2 |\delta\hat{\phi}_k|$ of the $n=0$ radial modes $[k_x=k, k_y=0]$ appears to be roughly in balance with the normalized linear growth rates $\hat{\gamma}(\vec{k})$ of the $n \neq 0$ peak driving modes $[k_x=0, k_y=k]$ (at least for low to moderate k). This provides a (normalized) saturation rule for the ($n=0$) radial modes: $|\delta\hat{\phi}(k_x)| \sim \hat{\gamma}(k_x)/\hat{k}_x^2$. This is similar to the often used rule for ($n \neq 0$) drift wave nonlinear saturation: $|\delta\hat{\phi}(k_y)| \sim \hat{\gamma}(k_y)/\hat{k}_y^2$. Conclusions (6)–(8) imply that the nonlinear transfer $E \times B$ shearing action of the radial modes is more important than dissipation in radial modes.

Finally, in *apparent* (if not actual) contradiction to previous work^{12,13} many of these findings (1)–(8) [and particularly “the paradigm,” i.e., (3) and (4)] appear to be universal, holding almost equally well for ITG-ae, mixed ITG/TEM, and purely TEM low- k turbulence, and in part even for ETG high- k turbulence, which has weaker zonal flow intensity relative to drift waves. An overall practical conclusion for the construction of quasilinear transport models is given in Sec. V: the drift wave turbulent intensity appears to be nearly linear in the GAM frequency.

II. ZONAL FLOW (LOW- q) VERSUS GAM (HIGH- q) SATURATION

It is now well known^{6,7} that for low- k ion scale turbulence (like ITG or TEM) $k_\perp \rho_s < 1$ (where $\rho_s = c_s/\Omega_i$, $c_s = \sqrt{T_e/M_i}$, and $\Omega_i = eB/cM_i$), the linear response of the potential for the $n=0$ radial modes (at $k_x \rho_s \rightarrow 0$) to an impulse

at $t=0$ can be decomposed into a residual (zero frequency) zonal flow with magnitude A_R and an oscillatory GAM with magnitude $(1-A_R)$:

$$\delta\phi(t)/\delta\phi(0) = A_R + (1-A_R)\cos(\omega_G t)\exp(-\gamma_G t), \quad (1)$$

where $A_R = 1/[1 + 1.6q_0^2/\varepsilon^{1/2}]$, $\gamma_G = \omega_G \exp(-q_0^2)$, and $\omega_G = \sqrt{7/4 + T_e/T_i}(v_{thi}/R_0)$, with $v_{thi} \equiv \sqrt{2T_i/M_i}$ and $\varepsilon \equiv r/R$. Formulas for larger residual at large $k_\perp \rho_s < 1$ can be found in Ref. 14. Physically $q_0 = q$ and $R_0 = R$, the values of the local safety factor and major radius seen by the $n \neq 0$ modes, but in the numerical experiments here, q_0 and R_0 are allowed to deviate from the physical values. (The R in the $\varepsilon \equiv r/R$ parameter for the radial modes remains fixed and physical.) At large q_0 , the zonal flow residual (A_R) decreases like $1/q_0^2$ and the GAMs dominate since their strong damping at low q_0 weakens rapidly as q_0 increases along with the increase in their excitation factor $1-A_R$. Note that in the original gyrofluid models,^{1,2} the radial modes were exponentially damped at a rate proportional to a curvature drift frequency $|k_x \rho_s|(c_s/R)$; hence, there were no GAMs and no zonal flow residual. The GAM damping rate has a similar (c_s/R) scaling but no linear wave number $|k_x \rho_s|$ dependence at small $|k_x \rho_s|$. It should be emphasized that the gyrofluid exponential decay model for the radial modes is very different from the impulse decay to a zero mean frequency zonal flow residual [Eq. (1)]. The usual working assumption following from the Hinton–Rosenbluth^{6,7} work has been that the *linear* zonal flow residual fraction A_R is the best indicator of the *nonlinear* radial modes shearing strength. As we will discuss, the relative efficiency of GAMs has generally been assumed small and the $1-A_R$ fraction ignored. Indeed the relative importance of zonal flows and GAMs is not easy to conclusively determine. The practical end to our quest is this: Should we associate a *nonlinear* reduction in transport due to increased shearing from radial modes to a decrease in the *linear* zonal flow residual fraction A_R and/or a decrease in *linear* the GAM damping rate γ_G or better the GAM frequency ω_G ? Fortunately, A_R , γ_G , and ω_G have very different dependences on q_0 and R_0 . We must keep in mind that both A_R and γ_G vanish at very high q_0 , whereas ω_G is independent of q_0 .

To best indicate the relative importance of zonal flow residuals versus GAMs in nonlinearly saturating the transport, we first consider the ITG-ae transport for the GA-standard case: $q=2$, $\hat{s} = d \ln q / d \ln r$, $R/a=3$, $r/a=1/2$, $T_i/T_e=1$, $n_i/n_e=1$, $a/L_T=3$, $a/L_n=1$ with $\alpha=0$ infinite aspect ratio circular s - α geometry. The unit of length a is the minor radius (r) of the last closed flux surface. For cases with kinetic electrons, we take $\mu = \sqrt{M_i/m_e}=60$, $\beta_e=0$, and $\nu_{ei}/[c_s/a]=0$. (Note that electron-ion collisions have little if any effect on radial modes since the electrons are nearly adiabatic. Ion-ion collisions can damp zonal flows and GAMs, but the $\nu_{ii}/[c_s/a]$ rates in tokamaks are too small to be significant.) The typical numerical parameters for these GYRO simulations are as follows: $[L_x/\rho_s, L_y/\rho_s]=[80, 105]$, $\Delta x/\rho_s=0.83$, 16 modes in $0 \leq k_y \rho_s \leq 0.90$ with 12 grids in the parallel direction, 15 in the gyroaverage, and 5 in the radial derivative; there are 128 velocity space grids per spatial cell

TABLE I. Ion energy diffusivity χ_i normalized to gyro-Bohm $\chi_{\text{gB}} = (c_s/a)\rho_s^2$ for the GA-standard case with variation of $n=0$ mode q_0 from $q=2$ and variation of R_0/a from $R/a=3$. The “ \pm ” indicates the sampling uncertainty (difference between the first half and second half compared to full overall time averages which captures any long time drift in the time average) and not the larger rms deviation from the overall mean which contains both the drift and the intermittency.)

q_0	R_0/a	ITG-ae	ITG/TEM		TEM2	
			χ_i/χ_{gB}	χ_e/χ_{gB}	χ_i/χ_{gB}	χ_e/χ_{gB}
1	3	2.81 ± 0.03	9.82 ± 0.07	2.92 ± 0.02	22.8 ± 0.4	26.6 ± 0.5
2 ($q_0=q$)	3 ($R_0=R$)	3.76 ± 0.06	12.06 ± 0.02	3.30 ± 0.04	25.2 ± 0.8	29.5 ± 0.9
6	3*	4.1 ± 0.2	13.5 ± 3.4	3.3 ± 0.2	27.4 ± 2.3	32.4 ± 2.7
12	3	4.82 ± 0.08	12.4 ± 1.7	3.0 ± 0.3	29.4 ± 0.7	34.9 ± 0.7
2	6	1.87 ± 0.1	3.6 ± 0.3	1.20 ± 0.06	14.8 ± 0.6	16.9 ± 0.7
3	6	1.99 ± 0.04	3.2 ± 0.2	0.96 ± 0.08	11.3 ± 0.8	12.7 ± 0.9
6	6*	1.5 ± 0.2	2.1 ± 0.1	0.58 ± 0.05	8.9 ± 0.3	9.9 ± 0.4

(eight energies, eight pitch angles, and two parallel directions). The statistical average values from the simulations were typically taken from time averages starting at $100[a/c_s]$ and lasting to $1000[a/c_s]$. These parameters are used unless otherwise stated. See the GYRO¹¹ website for extensive documentation. The code algorithms are largely unchanged since 2003 apart from new diagnostics indicated in this paper.

As shown in Table I, as q_0 increases from 1 to 12 past the GA-standard value $q=2$ with $R_0/a=R/a=3$ held fixed, the ITG-ae (third column) ion energy transport increases almost twofold from $q_0=1 \rightarrow 6$ even while the driving rates remain fixed. This would appear to indicate zonal flows are considerably more effective than GAMs for at least for limiting ITG-ae transport. (Transport energy diffusivities are normed to the gyro-Bohm diffusivity $\chi_{\text{gB}} = c_s \rho_s^2 / a$.) However, comparing the (*) cases with $q_0=6$, $R_0/a=3$ and $q_0=6$, $R_0/a=6$ at the same q_0 (or $q_0=3$, $R_0/a=6$ at the same $q_0 R_0/a$), it is also apparent that the GAMs could reduce the ITG-ae transport more than twofold if they could be slowed down by a factor (i.e., $\omega_G \rightarrow \omega_G/2$) or at low $q_0=2$ reducing their damping (i.e., $\gamma_G \rightarrow \gamma_G/2$) twofold (second and fifth columns). From Table I, ITG-ae transport is proportional to $\sim |\omega_G|$ at $q_0=2$ and $\sim |\omega_G|^{1.4}$ at $q_0=6$.

There are two arguments as to why the high frequency GAMs could be expected to be less effective than the zero mean frequency zonal flows: first, the oscillatory $E \times B$ shearing is less effective; second, the frequency mismatch between a triad of drift wave modes and GAM radial modes weakens the nonlinear coupling.

The first argument emphasizes the importance of toroidicity in $E \times B$ shear stabilization of drift waves.¹⁵ Note that based on equilibrium (steady state) long scale $E \times B$ shear stabilization, the shearing from the $n=0$ radial modes (with frequency ω_R) causes the most unstable outboard drift-ballooning mode at $\theta_0 = \theta = 0$ to rotate toward the inboard good curvature at $\theta = \pi$ with the speed¹⁵ $\partial \theta_0 / \partial t = \tilde{\gamma}_E(t) / \hat{s}$, where $\tilde{\gamma}_E(t) = \tilde{\gamma}_E^{\text{max}} \sin(\omega_R t)$ is the instantaneous $E \times B$ shear rate. While the residual zonal flows fluctuate, their effective frequency $\omega_R = \omega_{\text{ZF}}$ ($\omega_{\text{ZF}} < \Delta \omega_{\text{ZF}}$ their decorrelation rate) is very small and much smaller than for GAMs (where $\omega_R = \omega_G$ and $\Delta \omega_G \sim \Delta \omega_{\text{ZF}}$). The maximum possible swing in

the direction of good curvature (which lowers the effective driving rate of the unstable drift modes) for a GAM is $\Delta \theta^{\text{max}} = \pm \tilde{\gamma}_E^{\text{max}} / [\sqrt{2} \hat{s} \omega_G]$, whereas the swing is unlimited for a zonal flow. Thus, for the same $\tilde{\gamma}_E^{\text{max}}$ (same maximum amplitude of a given k_x radial mode), the GAM has a smaller swing in poloidal angle toward the good curvature and thus is less able to disrupt the formation of the most unstable linear eigenmode, which relies on the different poloidal harmonics [centered at rational surfaces where $q = \dots, (m-1)/n, m/n, (m+1)/n, \dots$] remaining in phase; i.e., outboard ballooning at $\theta=0$.

The second argument arises from the fact that the maximum amplitude of a given k_x radial mode (giving the $\tilde{\gamma}_E^{\text{max}}$) depends on how strongly it nonlinearly couples to the available drift waves. The strength of nonlinear coupling of a triad [$\vec{k}_R + \vec{k}_{\text{DW}} - \vec{k}_{\text{T-DW}} = 0$] is strongly reduced when the frequency mismatch $\omega_{\text{mis}} = \omega_R + \omega_{\text{DW}} - \omega_{\text{T-DW}}$ is much greater than sum of the decorrelation rates $\Delta \omega = \Delta \omega_{\text{DW}} + \Delta \omega_R + \Delta \omega_{\text{T-DW}}$,¹⁶ i.e., the interaction is “nonresonant.” Here, DW is an unstable $n > 0$ drift mode (with $k_{\text{xDW}} \sim 0$), T-DW is the less unstable (and possibly stable) “transfer” drift mode at the same n and $k_x = k_{\text{xR}} + k_{\text{xDW}}$, and R is the $n=0$ and $k_x = k_{\text{xR}}$ radial mode. Since $\omega_{\text{DW}} - \omega_{\text{T-DW}}$ is expected to be small due to weak radial dispersion, $\Delta \omega / \omega_{\text{mis}} \sim \Delta \omega / \omega_G \ll 1$ for GAMs, while $\Delta \omega / \omega_{\text{mis}} \sim \Delta \omega / \omega_Z \sim 1$ for residual zonal flows. This frequency mismatch argument is essentially equivalent to that of Hahm *et al.*,¹⁷ who argued the effective (time average) $E \times B$ shear rate of a radial mode with frequency ω_R (not necessarily the high frequency GAM) is reduced by $\Delta \omega_{\text{DW}} / \omega_R$, the ratio of drift wave decorrelation rate to the frequency of the radial mode.

Turning to the kinetic electron for the GA-standard case, the mixed ITG/TEM (fourth and fifth columns of Table I), and the purely trapped electron mode TEM2 case (sixth and seventh columns) with $a/L_T = 3 \rightarrow 1$ and $a/L_n = 1 \rightarrow 3$, we see a similar trend with increasing q_0 except that the effect of decreasing zonal flow residuals and GAM damping is not as strong as the ITG-ae case. Again, GAMs are shown to be more effective at limiting transport if they are artificially slowed down by $R_0 = R \rightarrow R_0 = 2R$. (The drift wave, zero mean frequency, and GAM frequency spectra for the ITG/TEM and

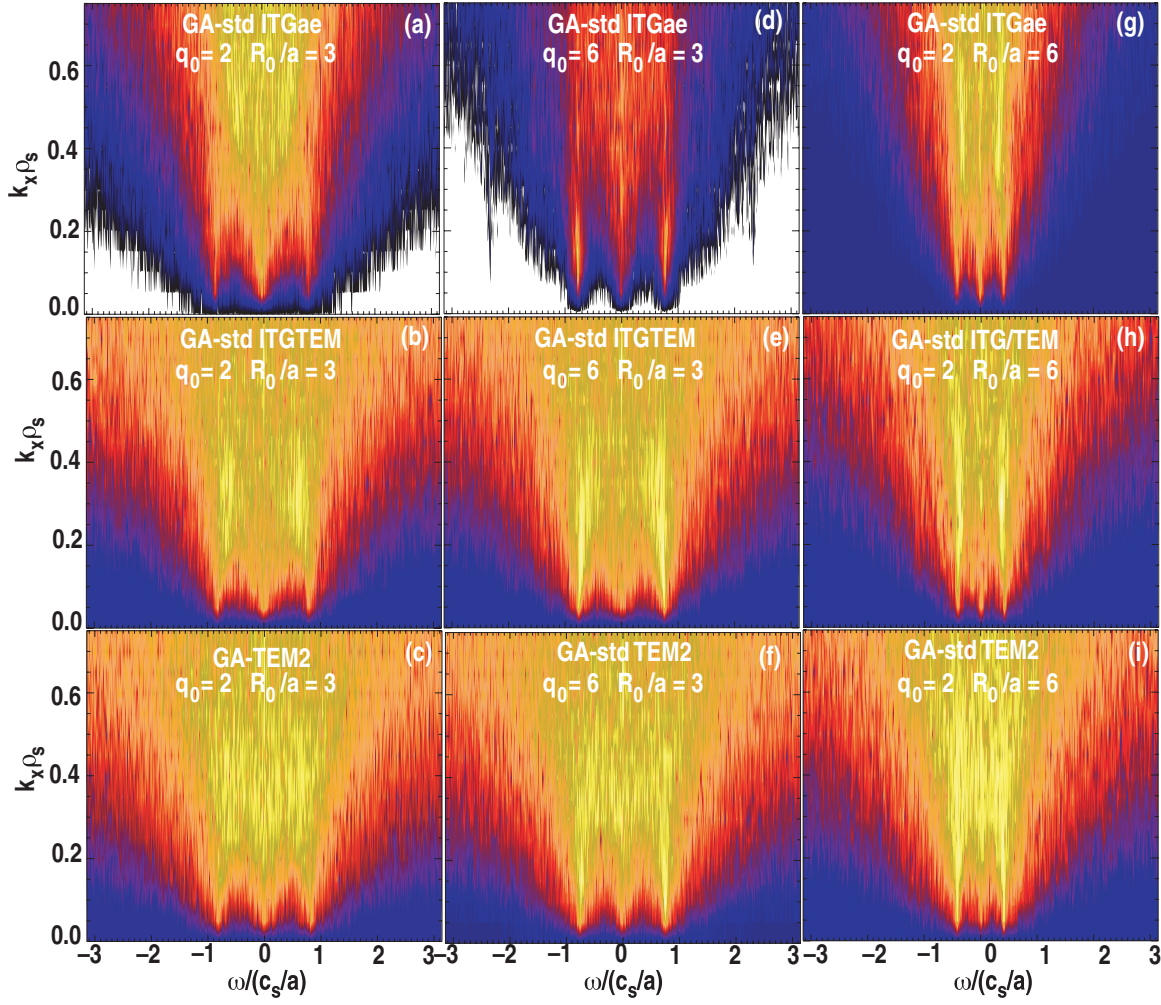


FIG. 1. (Color) Contour plots of the $[k_x, \omega]$ power spectrum of the radial mode shear rate $\log_{10} |\hat{k}_x^2 \delta \phi_k(\omega)|^2$ with $q_0=q$, $R_0=R$ [(a), (b), (c) left], $q_0=3q$, $R_0=R$ [(d), (e), (f) center], $q_0=q$, $R_0=2R$ [(g), (h), (i) right] for the GA-std ITG-ae [(a), (d), (g)], GA-std ITG/TEM [(b), (e), (h)], and GA-TEM2 [(c), (f), (i)] cases.

TEM2 cases are shown in Fig. 17 of Ref. 18.) To understand this contrast between the ITG-ae case and the ITG/TEM and TEM2 cases, Fig. 1 shows contour plots of the $[k_x, \omega]$ power spectrum of the radial mode shear rate which may be the best overall indicator of the relative importance of the zonal flow versus GAM fractions of the radial modes: the three base physical simulations ($q_0=q$ and $R_0=R$; i.e., second row of Table I) are in the left column, and the modified radial mode ($q_0=3q$ and $R_0=R$) simulations in the middle, and ($q_0=q$ and $R_0=2R$) simulations in rightmost column. Note that from the formula following Eq. (1), the GAM signature frequency appears at $\omega_G/[c_s/a]=0.77$ and half that for $R_0=2R$. As q_0 increase from 2 to 6, the *low-k intensity* (not shown) of the zonal flows decreases and the GAMs increase. However, most of the shearing is at high k . As Fig. 1 indicates, the kinetic electron cases (ITG/TEM and TEM2) start with much (at least half) of the shearing already in the GAMs ($\omega \sim \omega_G$) at both low $q_0=2$ and high $q_0=6$, whereas the ITG-ae case has most of the shearing in the high- k zonal flows ($\omega \sim 0$) and decreases as the residual decreases with increasing q_0 , allowing the GAMs to compete. At low $q_0=q=2$ with $R_0/a=R/a=3 \rightarrow R_0/a=6$, the GAM frequency (as well as damping) is cut in half, and the corresponding

rightmost column of Fig. 1 appears to indicate that shearing from GAMs dominates over that from the (zero mean frequency) zonal flows even for the ITG-ae case, and all cases comparing the second row of Table I with the fifth, the transport is more than cut in half. In all three cases in Fig. 1, when the zonal flow intensity is turned down and the GAM intensity up ($q_0=2 \rightarrow 6$ with $R_0=R$, i.e., contrasting the second with the third row in Table I), the power spectrum of the drift wave modes (at each k_y , summed over k_x) shows (not illustrated here) an undamped transfer drift mode at $\omega_{T-DW} = \omega_G + \omega_{DW}$ (nonlinearly generated by the GAMs) with almost equal intensity to the base drift mode at ω_{DW} (at each k_y , summed over k_x). The existence of this nonlinear pumped mode complicates (if not invalidates) the frequency mismatch *second* argument above (since the pumped mode has a very small mismatch). We hasten to add that Fig. 1 standing alone (without reference to the transport) only measures how the time average shearing rate is divided between low frequency (zonal flows) and high frequency (GAMs). It says nothing about the “effectiveness” of the high relative to low frequencies in limiting transport (i.e., the *first argument* given above).

It appears that the overall practical conclusion from

TABLE II. Ion (electron) energy diffusivity $\chi_i[\chi_e]$ normalized to gyro-Bohm $\chi_{gB}=(c_s/a)\rho_s^2$ for the GA-std case (ITG-ae, ITG/TEM), and the GA-TEM2 ($a/L_T=3 \rightarrow 1$, $a/L_n=1 \rightarrow 3$) case comparing full (all n) to various partial nonlinear coupling. Nonlinear conservation of entropy (see Sec III.) indicated by Y(es)/N(o). “Decoup $n \neq 0$ from $n=0$ ” in the third, fourth, and fifth rows means that the drift waves ($n \neq 0$) are not coupled to the radial modes ($n=0$) or a particular component of the radial modes. However, in all rows the radial modes are coupled to the drift waves. GYRO is spectral in n . The nonlinear term in each $n \neq 0$ drift wave is a simple convolution, so that decoupling from other modes (with $n=0$ in third, fourth, and fifth rows or with a different $n \neq 0$ in the second row) is simple to implement.

		ITG-ae	ITG/TEM		TEM2	
		χ_i/χ_{gB}	χ_i/χ_{gB}	χ_e/χ_{gB}	χ_i/χ_{gB}	χ_e/χ_{gB}
All n coupled	Y	3.52 ± 0.03	12.06 ± 0.02	3.30 ± 0.04	25.2 ± 0.8	29.5 ± 0.9
Each $n \neq 0$ to $n=0$ only	Y	4.55 ± 0.10	16.4 ± 1.53	7.60 ± 0.43	27.8 ± 1.1	30.1 ± 1.2
Decoup $n \neq 0$ from $n=0$ $\delta\phi$	Y	159 ± 70	956 ± 6	198 ± 5	359 ± 7	475 ± 12
Decoup $n \neq 0$ from $n=0$ δf	N	0.003	0.004	0.04	0.20 ± 0.07	0.17 ± 0.06
Decoup $n \neq 0$ from $n=0$	N	$l \arg e$	>300	>80	>300	>300

these numerical experiments, is that *the transport* [or essentially the drift wave ($n \neq 0$) intensity of the potential fluctuations] *is at least linearly (and some cases at high q_0 more than quadratically) proportional to the GAM frequency ($|\omega_G|$), which scales as a/R_0 .* (γ_G is also proportional to a/R_0 but since it is vanishingly small at high q_0 , we cannot say the drift wave intensity is proportional to γ_G .) The partition of an initial nonlinear pump impulse, A_R for zonal flows and $(1-A_R)$ for GAMs is effected by q_0 but independent of a/R_0 . While GAMs are more strongly damped at low q_0 , they still exist at low q_0 and their damping is weaker at smaller a/R_0 . Even at low q_0 , the high frequency GAMs appear to be equally if not more important than the zero mean frequency residuals in controlling the saturation level. The GAM damping rate sets the time scale to get to the zonal flow residual with smaller average amplitude relative to the initial pulse amplitude. In that sense the GAM damping rate (which at low q_0 is comparable to and scales as $|\omega_G|$) is an important element of the zonal flow physics even when the residual zonal flow component dominates the shearing.

III. COMPONENT PARTS OF THE NONLINEAR SATURATION MECHANISM

To determine what part of the nonlinear coupling between drift waves and zonal flows (radial modes) is most important, we delete parts of the *nonlinear coupling* while keeping both the $n \neq 0$ and the $n=0$ linear parts unchanged; i.e., $q_0=q$ and $R_0=R$. Table II summarizes the results for ITG and TEM cases. The first row is for full (all n) coupling. The second row is for each $n \neq 0$ coupled to $n=0$ only; i.e., every $n=n_1+n_2$ coupling triad which has $n \neq 0$, $n_1 \neq 0$, and $n_2 \neq 0$ (drift wave to drift wave) is deleted. Comparing the small difference in transport between the second and first rows for ITG-ae and TEM2 ($a/L_T=3 \rightarrow 1$, $a/L_n=1 \rightarrow 3$), the direct drift wave to drift wave coupling appears to be rather small but more significant in the mixed ITG/TEM case. The neglect of direct drift wave–drift wave coupling distorts the spectrum in all cases. In the third, fourth, and fifth rows, drift

wave to drift wave coupling is allowed, and the radial modes can couple to the drift waves. However, each drift wave is allowed to couple only to the radial mode ($-\delta f$) diamagnetic flow component in the third row, and only to the ($-\delta\phi$) $E \times B$ flow component in the fourth row, but decoupled completely from both radial mode components in the fifth row. As indicated in Table II, the nonlinear transfer (or coupling) conserves “energy” [or more appropriately incremental entropy (see Sec. IV)] in the first three rows but not in the fourth and fifth rows, where the drift waves are decoupled from the radial mode ($-\delta f$). The transport in the fifth row is much larger than in the first (or second), as expected from the paradigm. Typically, the transport is larger in the third row than the fifth, and the fourth row has negligible transport. We can conclude that the ($-\delta\phi$) $E \times B$ shearing component is stabilizing (as expected from the paradigm) but the ($-\delta f$) diamagnetic shearing component are destabilizing. In essence, the diamagnetic zonal flows add to the driving temperature and density gradients at one location while subtracting at another: the additions dominate since the subtraction likely carry below a threshold. It would appear also that the *drift wave–zonal flow paradigm* for nonlinear saturation originally derived from (gyrofluid) ITG-ae simulations also applies to kinetic electrons: the ITG/TEM case is a mixed case with ion (ITG) directed modes at low k and electron (TEM) directed modes at high k ($k_y \rho_s \geq 0.5$); the TEM2 case with much higher density gradients and much lower temperature gradients has only trapped electron modes.

The close comparison of the first row (full coupling) with the second row (drift wave to drift wave coupling deleted) appears to be the best quantifiable evidence that drift wave to radial mode coupling dominates the nonlinear saturation (the main point of the *drift wave–zonal flow paradigm*). This is consistent with the (often observed but unpublished) fact that “two-mode” simulations (one $n \neq 0$ drift wave and the $n=0$ radial mode) often give close to the correct transport (if the single $k_y \rho_s$ is judiciously chosen). Furthermore, the drift wave with drift wave coupling strength is

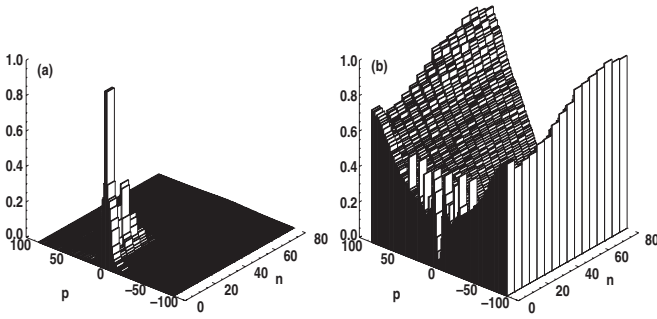


FIG. 2. $[\hat{k}_y(n), \hat{k}_x(p)]$ wave number spectral plots of mode amplitudes $|\delta\hat{\phi}_k|$ (a) and $E \times B$ shear rates $\hat{k}_x^2 |\delta\hat{\phi}_k|$ (b) for the GA-std ITG/TEM full coupling case. The wave number grid span $0 \leq \hat{k}_y(n) \leq 0.75$ and $-4.2 \leq \hat{k}_x(p) \leq 4.2$.

weaker than drift wave with radial mode by the nature of the $E \times B$ nonlinearity: $\hat{e}_z \cdot \hat{k}_1 \times \hat{k}_2 = |\hat{k}_1| |\hat{k}_2| \sin \Delta\theta_{12}$ with $\sin \Delta\theta_{12}$ larger for the latter. Figure 2 illustrates (for the ITG/TEM full coupling case) that although per mode, the radial mode amplitudes $|\delta\hat{\phi}_k|$ [Fig. 2(a)] tend to be larger than the drift wave amplitudes [owing to their low “inertia,” $\sim \hat{k}_x^2$ compared to $\sim (1 + \hat{k}_x^2 + \hat{k}_y^2)$; see Eqs. (2) and (3) below], they also have more $E \times B$ shear rate $\hat{k}_x^2 |\delta\hat{\phi}_k|$ [Fig. 2(b)] particularly at low \hat{k}_x . We hasten to add that deletion of the drift wave to drift wave coupling greatly distorts the \hat{k}_y spectrum of the drift wave turbulence and transport and there is no suggestion that it is a useful approximation.

Previous work^{12,13} on purely trapped electron mode turbulence appears to call into question the universality of the drift wave–zonal flow paradigm. Reference 12 considered a case similar to the TEM2 case: $q=2 \rightarrow 1.4$, $\hat{s}=1 \rightarrow 0.8$, $\mu=60 \rightarrow 20$, $a/L_n=3 \rightarrow 1$, $a/L_{T_i}=1 \rightarrow 0$, $a/L_{T_e}=1 \rightarrow 2$, and perhaps most importantly, $T_e/T_i=1 \rightarrow 3$. “Artificially suppressed” zonal flows had little effect on the transport.¹² Similarly, Ref. 13 considered $q=2 \rightarrow 1.4$, $\hat{s}=1 \rightarrow 0.8$, $\mu=60 \rightarrow 42$, $a/L_n=3 \rightarrow 3.3$, $a/L_{T_i}=1 \rightarrow 0$ with a scan $a/L_{T_e}=1 \rightarrow [0:3.3]$ and $T_e/T_i=1 \rightarrow [0.5:3.5]$ to find that when zonal flows were “zeroed out” the transport increased at “least 2.5-fold” for $T_e/T_i < 2.0$, but found “less than a 30% increase” for $T_e/T_i > 2.5$ for $a/L_{T_e} > 2$. Reference 13 used a larger a/L_n than Ref. 12, but the large $T_e/T_i=3$ appeared to be in agreement with Ref. 12. The $T_e/T_i=1$ results of Ref. 13 are not inconsistent with the TEM2 results in Table II, which indicate tenfold increases in the fifth row when drift waves are decoupled from radial modes). In Table III, we have repeated the TEM2 parameters with colder ions: $T_e/T_i=3$. It appears again that the drift wave–drift wave coupling is still responsible for most of the nonlinear saturation. Decoupling the drift waves ($n \neq 0$) from the zonal flows ($n=0$) [while still keeping the zonal flows coupled to (or pumped by) the drift waves] still results in a sevenfold increase (in contrast to the tenfold increase for $T_e/T_i=1$). However, contrasting the first row with the second in Table II and III, we see that deleting drift wave–drift wave coupling causes has almost no effect on the $T_e/T_i=1$ diffusivities, but for $T_e/T_i=3$ (Table III) the diffusivities decrease by half rather than increase (at least somewhat) in all other cases in Table II; i.e., cold ion TEM2

TABLE III. Ion (electron) energy diffusivity $\chi_i[\chi_e]$ normalized to gyro-Bohm $\chi_{GB}=(c_s/a)\rho_s^2$ for the GA-TEM2 ($a/L_T=3 \rightarrow 1$, $a/L_n=1 \rightarrow 3$) case except $T_e/T_i=1 \rightarrow 3$, comparing full (all n) to various partial nonlinear coupling. See the caption of similar Table II for detailed explanation of coupling and decoupling.

	TEM2 $T_e/T_i=1 \rightarrow 3$	
	χ_i/χ_{GB}	χ_e/χ_{GB}
All n coupled	20.6 ± 0.6	23.2 ± 0.7
Each $n \neq 0$ to $n=0$ only	14.1 ± 0.5	12.1 ± 0.5
Decoupled $n \neq 0$ from $n=0$	$>135 \pm 18$	$>169 \pm 25$

case is somewhat inconsistent with the others. This would appear to mean that the drift wave–drift wave coupling cannot be neglected for the cold ion TEM2 case. In this limited sense we are in partial agreement with Refs. 12 and 13. Note that the cold ion TEM2 diffusivities are less than the warm ion TEM2 diffusivity with full coupling and considerably less when the drift waves are coupled only to the radial modes. This is consistent with slowing down the GAMs by $\sqrt{3}=1.73$ -fold, which we have seen in Sec. II proportionally decreases the transport.

It seems any differences with Refs. 12 and 13 (that cold ion TEM is the exception to the paradigm or not) are less likely to do with precise differences in parameters and more likely do with the difference between *decoupling from* radial modes (as here) and *suppressing*¹² (or *zeroing out*)¹³ the $E \times B$ shear from zonal flows; the latter directly interrupts the linear evolution of the $n=0$ providing additional damping and a linear sink, whereas the former directly preserves nonlinear conservation and the linear evolution with no added sink and only indirectly effects the nonlinear pumping of the zonal flows (which may actually gets stronger). *Suppressing*¹² (or *zeroing out*)¹³ the $E \times B$ shear from radial modes, not only interrupts the GAMs, but the shear in the diamagnetic components remains.

Historically, transport from electron temperature gradient modes with adiabatic ions (ETG-ai) was considered isomorphic to ITG-ae transport: at the same plasma and magnetic profile parameters, the diffusivities need only be normalized by electron rather ion gyro-Bohm scaling $\chi_{GB}^e/\chi_{GB}^i=1/\mu$, with wave numbers and growth rates μ times larger and gyroradii μ times smaller. However, as first noted by Jenko and Dorland,¹⁹ while the drift wave physics is isomorphic (same normalized linear growth rates), the zonal flow physics is not and this results in an *order of magnitude* larger electron gyro-Bohm normalized ETG transport compared to ion gyro-Bohm normalized ITG-ae (roughly 16 times larger from Ref. 19). The isomorphy is broken by the density response for the adiabatic species: $\delta n^{\text{adia}}/n_0 = \lambda(e\delta\phi/T)$. For ITG-ae, $\lambda \sim 0$, since $n=0$ zonal flow electrons go adiabatic by parallel (along the field line) motion. For ETG-ai, $\lambda=1$, since ions go adiabatic by gyromotion (across field line motion) at ETG wave numbers ($k\rho_s > 1$). Note that in common practice gyrokinetic ETG-ai simula-

TABLE IV. Diffusivity χ normalized to gyro-Bohm $\chi_{\text{gB}} = (c_s/a)\rho_s^2$ for the GA-std case (with $\hat{s}=1 \rightarrow 0.2$) at various $n=0$ adiabaticity coefficient λ and comparing coupling with each $n \neq 0$ to $n=0$ only (last row) to full coupling (first row).

	$\lambda \sim 0$ ITG-ae	$\lambda=0.2$	$\lambda=0.4$	$\lambda=0.6$	$\lambda=0.8$	$\lambda=1.0$ ETG-ai
All n coupl	1.9 ± 0.1	2.7 ± 0.1	4.3 ± 0.1	7.1 ± 0.4	14.2 ± 0.7	37.0 ± 3.7
Each $n \neq 0$ to $n=0$ only	1.7 ± 0.1	2.52 ± 0.04	3.5 ± 0.3	5.4 ± 0.2	8.2 ± 0.5	14.3 ± 0.2

tions are actually ITG-ae simulations with $\lambda=1$ in place of $\lambda \sim 0$ (actually $[1 - \langle \delta\phi \rangle / \delta\phi]$). It is interesting to note that extending Ref. 7 to nonzero λ , the generalized zonal flow residual²⁰ is

$$\delta\phi_k(t \rightarrow \infty) / \delta\phi_k(0^+) = [\lambda + k_x^2 \rho_s^2] / [\lambda + k_x^2 \rho_s^2 (1 + 1.6q^2 / \varepsilon^{1/2})]. \quad (2)$$

The residual is 6.8 times (at $k_x \rho_s = 0.3$) [15 times (at $k_x \rho_s = 0.1$)] larger for ETG-ai compared to ITG-ae (which would *seem* to argue for relatively smaller ETG-ai transport); *however*, the important point is that the $n=0$ zonal flow “inertia” $[\lambda + k_x^2 \rho_s^2 (1 + 1.6q^2 / \varepsilon^{1/2})]$,

$$[\lambda + k_x^2 \rho_s^2 (1 + 1.6q^2 / \varepsilon^{1/2})] \partial(e \delta\phi_k / T) / \partial t = P_0(t) [c_s / a] [\rho_s / a], \quad (3)$$

is 1.6 times (at $k_x \rho_s = 0.3$) [6.9 times (at $k_x \rho_s = 0.1$)] i.e., up to an *order of magnitude* larger. To get the same $E \times B$ rate from the zonal flows, the pump strength from the drift waves P_0 must be an *order of magnitude* larger to match the larger inertia. It is instructive to note (as we demonstrate in Sec. IV for ITG-ai) that nonlinear saturation is achieved when the $E \times B$ shear rate of the zonal flows is about equal to the normalized growth rates of the unstable finite- n modes. Since the normalized growth rates for ITG-ae and ETG-ai are equal (isomorphic), this means that the $I = |(e \delta\phi / T) / (\rho_s / a)|^2$ normalized intensity of the ITG-ae and ETG-ai zonal flows are about equal. To get the order of magnitude larger pump strength P_0 , the average ETG-ai $n \neq 0$ drift wave normalized intensity (and transport) must be roughly an *order of magnitude* smaller. Hence, the ratio of zonal flow to drift wave average intensity ($I_{n \neq 0} / I_0$) is roughly an *order of magnitude* smaller for ETG-ai compared to ITG-ae. Only in this sense are ETG-ai zonal flows *weaker*.

These arguments for the relative strength of ETG-ai and ITG-ae transport and turbulence hang together only if the *drift wave–zonal flow paradigm* holds independent of λ from ITG-ae to ETG-ai and drift wave–zonal flow nonlinear coupling dominates over drift wave–drift wave nonlinear coupling. Table IV scanning λ from ITG-ae to ETG-ai for the GA-standard case (with $\hat{s}=1 \rightarrow 0.2$). As expected, the normalized transport (first numerical row) increases as λ approaches 1. If the $n \neq 0$ modes are decoupled from $n=0$, there is no definitive saturation and the transport is unphysically large (not shown in table); in that sense the paradigm holds equally well for ETG-ai turbulence. However, if only each $n \neq 0$ to $n=0$ couplings are allowed (second row of Table IV and the direct drift wave–drift wave coupling de-

leted, the increase in transport as λ approaches 1 is considerably less as compared with full all- n coupling (first row). Thus, direct drift wave–drift wave coupling is relatively more important for ETG-ai than for ITG-ae nonlinear saturation (where it is almost negligible in this case). This is consistent with the earlier argument that if the normalized ETG-ai transport is $O(10)$ -fold larger than ITG-ae, the ratio of drift wave to zonal flow amplitudes is expected to be $O(\sqrt{10})$ -fold larger. The argument relies on the normalized radial mode amplitude remaining approximately invariant with λ (radial mode shear rates need only match the linear growth rates, which are independent of λ); that is indeed the case for the simulations of Table IV.

The reader will note that we lowered the shear ($\hat{s}=1 \rightarrow 0.2$) in the λ for Table IV. It was shown in Ref. 21 that when trapping is included (as is the case in Table IV), $\lambda=1$ (i.e., ETG-ai) transport is indeterminately large at moderate to large shear ($\hat{s} > 0.4$), but ETG simulations with kinetic ions (ETG-ki) or ETG-ai with a very small level of additional equilibrium $E \times B$ shear²² is well behaved. The coupled ITG/TEM-ETG-ki simulations of Ref. 23 showed that most of the ETG (defined by $k_y \rho_s > 1$) electron transport accumulates at rather low k , suggesting that nearly ion scale zonal flows (effectively, $0 < \lambda < 1$) rather than high- k electron scale zonal flows may physically account for ETG transport saturation. Note ions are only about 50% (80%) adiabatic at $k_\perp \rho_s = 1(2)$ (Ref. 23), suggesting $\lambda=0.50$ (0.80) at the near ion scale.

IV. SPECTRUM OF NONLINEAR ENTROPY TRANSFER RATES AND THE ZONAL FLOW SATURATION RULE

To understand and quantify the nonlinear turbulence spectrum in the $[k_y, k_x]$ wave number space, it is useful to deal with the *conserved nonlinear transfer of the incremental entropy* spectrum $S_k = \langle \sum_s \int d\nu^3 n_0^s \hat{T}_0^s F_0^s | \delta f_k^s |^2 / 2 \rangle$, where $\langle \rangle$ is a flux surface average, s is the species label, \hat{T}_0^s is the species temperature (normed to the electron temperature), and F_0^s is the background Maxwellian distribution. The normalized perturbations in the distribution is $\delta f_k^s = \delta f_k^s / F_0^s$, where $F = \delta f + F_0$. The relation of $S = \sum_k S_k$ to usual sum over $F \ln(F/F_0)$ total entropy along with the details of following nonlinear entropy conservation can be found in Ref. 24. On time average steady state

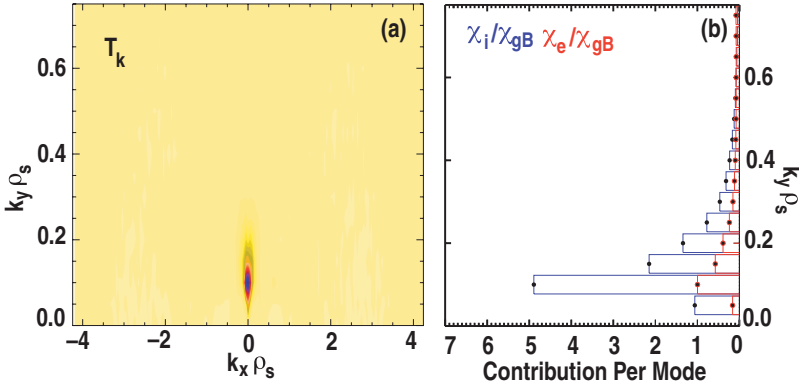


FIG. 3. (Color) (a) Contours of nonlinear entropy transfer spectrum with blue negative and yellow positive. (b) Coincident ion (blue) and electron (red) energy diffusivity $k_y \rho_s$ spectrum (integrated over $k_x \rho_s$). Both for the GA-std ITG/TEM case (columns 4 and 5 of Table II).

$$\begin{aligned} \partial[S + W]/\partial t = & \sum_{\vec{k}} T_{\vec{k}} + \sum_{\vec{k}} \left[\sum_s n_0^s \hat{T}_0^s \chi_{\vec{k}}^s / \chi_{gB}^s \right] (a/L_T^s)^2 \\ & + \sum_{\vec{k}} D_{\vec{k}}^{\text{dissip}} = 0, \end{aligned} \quad (4)$$

where $W = \langle \int d\nu^3 n_0^i F_0^i \sum_{\vec{k}} [\delta \hat{\phi}_{\vec{k}}^* G_{\vec{k}} \{ \delta \hat{\phi}_{\vec{k}} \}] / 2 \rangle$ and $G_{\vec{k}} \sim k_{\perp}^2 \rho_s^2$ is a kind of field entropy. {The rate unit is $[c_s/a]$ and $\delta \hat{\phi} = (e \delta \phi / T_e) / (\rho_s / a)$.} The details of the dissipation (see Ref. 24) need not concern us, except that it is broken into Landau damping along the field line and a high- k_x “numerical” dissipation representing collisional dissipation at very fine scales. $\sum_{\vec{k}} T_{\vec{k}} = 0$, where the *conserved nonlinear transfer* is $T_{\vec{k}} = \langle \sum_s \int d\nu^3 \hat{T}_0^s F_0^s \text{Re}[\delta \hat{f}_{\vec{k}}^{s*} [\delta \hat{v}_E \cdot \hat{\nabla} \delta \hat{f}_{\vec{k}}^s]] \rangle$. From Eq. (4), we can then define the steady state entropy transfer rate $2\gamma_{\vec{k}}^S$ (defined with the “2” because $S_{\vec{k}}$ is bilinear):

$$2\gamma_{\vec{k}}^S S_{\vec{k}} \equiv -T_{\vec{k}} = \sum_s n_0^s \hat{T}_0^s [\chi_{\vec{k}}^s / \chi_{gB}^s] (a/L_T^s)^2 + D_{\vec{k}}^{\text{dissip}}. \quad (5)$$

Direct computation of $S_{\vec{k}}$ and $T_{\vec{k}}$ are now included in GYRO simulations. As expected, the energy transport spectrum $[\chi_{\vec{k}}^s / \chi_{gB}^s]$ coincides with the entropy generation spectrum as illustrated with the GA-standard ITG/TEM case in Fig. 3. In effect, the peak *nonlinear transfer* T_k [Fig. 3(a)] *drains away* from the coinciding peak transport production [Fig. 3(b)] of entropy near $[k_y, k_x] \approx [0.1, 0.0]$ and *spreads* entropy evenly over the high- k_x dissipation modes. Figure 4 shows the contours for the *rate of entropy generation* less dissipation. The peak rate of production (yellow-orange) is at $[k_y, k_x] \approx [0.2, 0.0]$, which is *downshifted* from the peak growth rate at $[k_y, k_x] \approx [0.3, 0.0]$. The key point of Fig. 4 is that the *dissipation rate* (red-blue) is *spread evenly* over all n modes (all k_y) with no distinction between drift waves ($n \neq 0$) and radial modes ($n=0$). This indicates that the principal action of the radial modes $[k_y^R=0, k_x^R \neq 0]$ is the $(E \times B)$ shearing) nonlinear transfer of entropy generated in the drift wave at $[k_y^{\text{DW}} \neq 0, k_x^{\text{DW}}=0]$ to be dissipated in the transfer drift wave $[k_y^{\text{T-DW}}=k_y^{\text{DW}}, k_x^{\text{T-DW}}=k_x^R]$. Radial modes are not the principal source of dissipation. (The curious positive islands along $k_x = s k_y 2\pi$ in Fig. 4 correspond to the along the field extended poloidal angle $\theta=2\pi$ ballooning mode re-occurrences.)

We note in passing that contours of a similar nonlinear transfer function (broken into x and y $E \times B$ velocity shear-

ing) defined in the frequency domain was treated with GYRO in Ref. 8. Because GAMs have a distinctive frequency (with little dispersion), the nonlinear interaction between drift waves and GAMs is easily displayed in both simulations and experimental diagnostics.

In Fig. 5, we slice through Fig. 4 contours of the entropy rate $2\gamma_{\vec{k}}^S$ along the k_y axis [Fig. 5(a)] and along the k_x axis [Fig. 5(b)] to illustrate the effect of turning off the Landau damping (in all n). This is done in GYRO by setting the “up-winding” dissipation in the parallel derivative to zero. Without Landau damping, GAMs re-occur¹¹ and effectively, the zonal residual never obtains [see Eq. (1) with $\gamma_G=0$]. Note that the dissipation rate of the most important radial modes with $k_x \rho_s < 1$ is entirely due to Landau damping. As shown in Table V, the transport levels are remarkably insensitive to Landau damping. Without explicit collisions (the case here), if the additional high- k_x dissipation in GYRO were shut off, no stationary state could be obtained per Eq. (5).²⁴ It is important to emphasize, as shown in Ref. 24, that the transport is also quite insensitive to the details of the artificial high- k_x

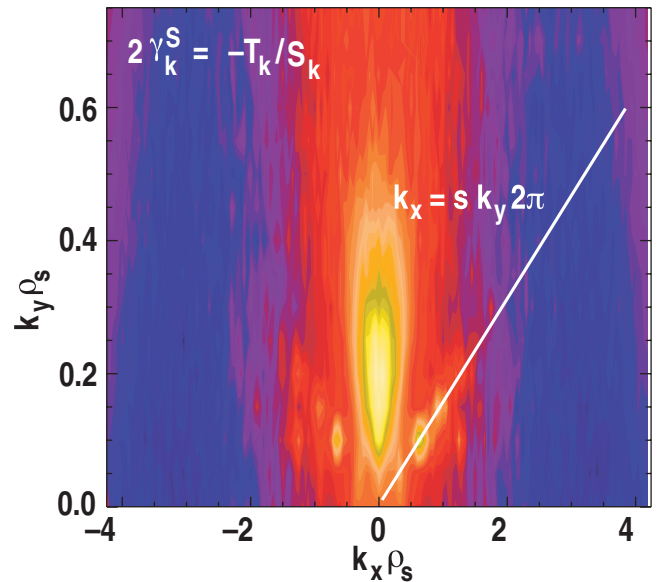


FIG. 4. (Color) Contours of nonlinear entropy transfer rate spectrum ($2\gamma_{\vec{k}}^S = -T_{\vec{k}}/S_{\vec{k}}$) with blue negative and yellow positive (otherwise same as Fig. 1). The zero contour separates orange (slightly positive) from red (slightly negative).

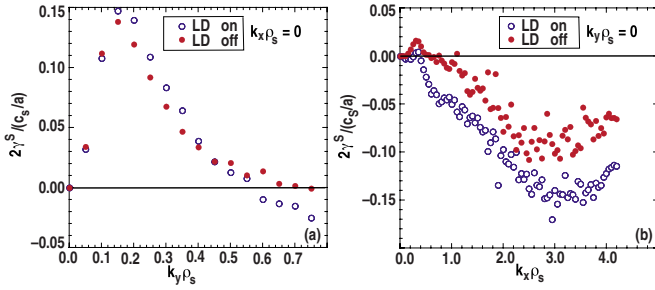


FIG. 5. (Color online) Nonlinear entropy transfer rate spectrum ($2\gamma_k^S = -T_k/S_k$) along the k_y axis in (a) and along the k_x axis in (b). With (open blue circles) [without (closed red circles)] Landau damping.

damping which dissipates the entropy at small scales, while leaving the large scales which drive the transport unaffected.

For the three cases considered in Table II, Fig. 6 quantifies the often observed rule (e.g., Ref. 13) that *rms zonal flow shear rates are in balance with the drift wave linear growth rates*: $\tilde{\gamma}_E(\hat{k}_y=0, \hat{k}_x=\hat{k}) \sim (1.0 \pm 0.5) \hat{\gamma}^{\text{linear}}(\hat{k}_y=\hat{k}, \hat{k}_x=0)$. [From Fig. 6(c), the TEM2 warm ion case has the larger deviations from this rule: $\tilde{\gamma}_E \sim 0.5 \hat{\gamma}^{\text{linear}}$.] Reference 13 found $\tilde{\gamma}_E \sim \hat{\gamma}^{\text{linear}}$ for a similar warm ion case but $\tilde{\gamma}_E \sim 0.2 \hat{\gamma}^{\text{linear}}$ for cold a similar cold ion case.) Hence, by definition of the rms $E \times B$ shear rate $|\delta\hat{\phi}|(\hat{k}_y=0, \hat{k}_x=\hat{k}) \sim (1 \pm 0.5) \hat{\gamma}^{\text{linear}}(\hat{k}_y=\hat{k}, \hat{k}_x=0)/\hat{k}_x^2$, where $\hat{k} = k\rho_s$. This provides a zonal flow saturation rule similar to the often used²⁵ drift wave saturation rule: $|\delta\hat{\phi}|(\hat{k}_y=\hat{k}, \hat{k}_x=0) \propto \hat{\gamma}^{\text{linear}}(\hat{k}_y=\hat{k}, \hat{k}_x=0)/\hat{k}_y^2$ to which we return below. Clearly, this is unlikely to be the most accurate saturation rule, as it does not make reference to the radial mode physics, which is now well known to control the nonlinear saturation.

V. CONCLUSION

Our overall practical conclusion serves to guide the construction of theory based local gyroBohm scaled transport models. The most successful currently used models (e.g., MultiMode,²⁵ GLF23,²⁶ or TGLF²⁷) take the transport from the few most unstable drift waves each wave number $\hat{k}_y(\hat{k}_x=0)$ to be given by the product of a quasilinear weight W_k^{QL} and a nonlinear saturation rule for a drift wave spectral intensity like $|\delta\hat{\phi}_k|^2$. W_k^{QL} is derived precisely from the drift wave eigenmodes of the linear fluid,²⁵ gyrofluid,^{26,27} or, in principle, gyrokinetic equations. There is no precise derivation for the drift wave spectral intensity which must rely on heuristic formulas best fitted to gyrofluid²⁶ or better gyrokinetic simulations.²⁷ From dimensional constraints and the form of the nonlinear $E \times B$ coupling, heuristic reasoning

TABLE V. Transport diffusivities normed to gyro-Bohm for GA-std ITG/TEM case (in Fig. 3) with (without) Landau damping.

Landau damping	χ_i/χ_{gB}	χ_e/χ_{gB}	D_e/χ_{gB}
With	11.82	3.27	-1.99
Without	13.17	3.55	-1.80

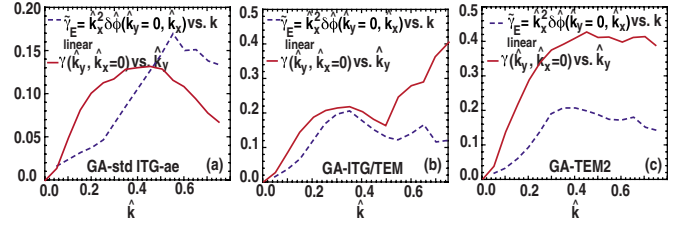


FIG. 6. (Color online) Zonal flow $E \times B$ shear rates (dashed blue lines) and drift wave growth rates (in $[c_s/a]$ units) (solid red lines) vs wave number $\hat{k} = k\rho_s$ for the GA-std ITG-ae (a); ITG/TEM (b); TEM2 (c) cases of Table II.

suggests $|\delta\hat{\phi}_k| = \hat{C}(\hat{\gamma}_k^{\text{linear}})^{\alpha}(\hat{\gamma}_k^X)^{(1-\alpha)}/\hat{k}_y^2$. MultiMode²⁵ takes $\alpha=1$ and C form an experimental fit. In principle, $\hat{\gamma}_k^X$ could be any rate (or absolute frequency). From the “predator (zonal flow)–prey (drift wave)” concept,³ GLF23²⁶ took $\hat{\gamma}_k^X$ to be a gyrofluid radial mode damping rate proportional to $|\hat{\omega}_k^D| \sim (a/R)(k_y\rho_s)$ (assuming $k_x^R \sim k_y^{\text{DW}}$) with the best fit to gyrofluid simulations $\alpha \sim 1/2$. The TGLF model²⁷ continued this curvature drift frequency scaling with a stronger with α exponent.

This paper suggest that the importance of GAM physics relative to the size and significance of the zonal flow residual A_R [see Eq. (1)] has been underappreciated in previous work. While the GAM damping rate $\hat{\gamma}_G$ also sets the time scale to form the zonal flow residual from an initial pulse, it nearly vanishes at high q . Since the transport does not vanish at high q (in fact it increases), this strongly suggests that the GAM frequency $|\hat{\omega}_G|$ (rather than the similar $|\hat{\omega}_k^D|$) provides a more physically motivated and accurate choice for $\hat{\gamma}_k^X$ in the nonlinear saturation rule (simulations in Sec. II suggest $1/2 \leq \alpha < 1$). While these rates are similar in their (a/R) dependence to the curvature drift frequency rate (used in GLF23 and TGLF), they have no strong $k_y\rho_s$ dependence. Their use would provide a drift wave spectral intensity with a faster falloff to higher $k_y\rho_s$.

ACKNOWLEDGMENTS

We thank Dr. Jeff Candy for discussions on how to define the entropy transfer rate and Dr. G. M. Staebler for many discussions on heuristic formulas for nonlinear saturation rules.

This work was supported by the U.S. Department of Energy under Cooperative Agreement Nos. DE-FC02-04ER54698 and DE-FG02-07ER54917.

¹G. W. Hammett, M. A. Beer, W. Dorland, S. C. Cowley, and S. A. Smith, *Plasma Phys. Controlled Fusion* **35**, 973 (1993).

²R. E. Waltz, G. R. Kerbel, and J. Milovich, *Phys. Plasmas* **1**, 2229 (1994).

³P. H. Diamond, S.-I. Itoh, K. Itoh, and T. S. Hahm, *Plasma Phys. Controlled Fusion* **47**, R35 (2005).

⁴A. M. Dimits, B. I. Cohen, W. M. Nevins, and D. E. Shumaker, *Nucl. Fusion* **40**, 1725 (2001).

⁵R. E. Waltz, M. E. Austin, K. H. Burrell, and J. Candy, *Phys. Plasmas* **13**, 052301 (2006).

⁶F. L. Hinton and M. N. Rosenbluth, *Plasma Phys. Controlled Fusion* **41**, A653 (1999).

⁷M. N. Rosenbluth and F. L. Hinton, *Phys. Rev. Lett.* **80**, 724 (1998).

⁸R. C. Holland, G. R. Tynan, R. J. Fonck, G. R. McKee, J. Candy, and R. E. Waltz, *Phys. Plasmas* **14**, 056112 (2007).

⁹A. Fujisawa, T. Ido, A. Shimizu, S. Okamura, K. Matsuoka, H. Iguchi, Y.

- Hamada, H. Nakano, S. Ohshima, K. Itoh, K. Hoshino, K. Shinohara, Y. Miura, Y. Nagashima, S.-I. Itoh, M. Shats, H. Xia, J. Q. Dong, L. W. Yan, K. J. Zhao, G. D. Conway, U. Stroth, A. V. Melnikov, L. G. Eliseev, S. E. Lysenko, S. V. Perfilov, C. Hidalgo, G. R. Tynan, C. Holland, P. H. Diamond, G. R. McKee, R. J. Fonck, D. K. Gupta, and P. M. Schoch, *Nucl. Fusion* **47**, S718 (2007).
- ¹⁰D. K. Gupta, R. J. Fonck, G. R. McKee, D. J. Schlossberg, and M. W. Schafer, *Phys. Rev. Lett.* **97**, 125002 (2006).
- ¹¹J. Candy and R. E. Waltz, *J. Comput. Phys.* **186**, 545 (2003); see also *Phys. Rev. Lett.* **91**, 045001 (2003) and the GYRO website: <http://fusion.gat.com/theory/Gyro>.
- ¹²T. Dannert and F. Jenko, *Phys. Plasmas* **12**, 072309 (2005).
- ¹³J. Lang, S. E. Parker, and Y. Chen, *Phys. Plasmas* **15**, 055907 (2008).
- ¹⁴Y. Xiao and P. J. Catto, *Phys. Plasmas* **13**, 102311 (2006).
- ¹⁵R. E. Waltz, R. L. Dewar, and X. Garbet, *Phys. Plasmas* **5**, 1784 (1998).
- ¹⁶R. E. Waltz, *Phys. Fluids* **26**, 168 (1983).
- ¹⁷T. S. Hahm, M. A. Beer, Z. Lin, G. W. Hammett, W. W. Lee, and W. M. Tang, *Phys. Plasmas* **6**, 922 (1999).
- ¹⁸J. E. Kinsey, R. E. Waltz, and J. Candy, *Phys. Plasmas* **13**, 022305 (2006).
- ¹⁹F. Jenko, W. Dorland, M. Kotschenreuther, and B. N. Rogers, *Phys. Plasmas* **7**, 1904 (2000).
- ²⁰E.-J. Kim, C. Holland, and P. H. Diamond, *Phys. Rev. Lett.* **91**, 075003 (2003).
- ²¹W. M. Nevins, S. E. Parker, Y. Chen, J. Candy, A. Dimits, W. Dorland, G. W. Hammett, and F. Jenko, *Phys. Plasmas* **14**, 084501 (2007).
- ²²J. Candy, R. E. Waltz, M. Fahey, and C. Holland, *Plasma Phys. Controlled Fusion* **49**, 1209 (2007).
- ²³R. E. Waltz, J. Candy, and M. Fahey, *Phys. Plasmas* **14**, 056116 (2007).
- ²⁴J. Candy and R. E. Waltz, *Phys. Plasmas* **13**, 032310 (2006).
- ²⁵J. E. Kinsey and G. Bateman, *Phys. Plasmas* **3**, 3344 (1996).
- ²⁶R. E. Waltz, G. M. Staebler, G. W. Hammett, M. Kotschenreuther, and J. A. Konings, *Phys. Plasmas* **4**, 2482 (1997).
- ²⁷G. M. Staebler, J. E. Kinsey and R. E. Waltz, *Phys. Plasmas* **14**, 055909 (2007), APS06 issue; see also J. E. Kinsey, G. M. Staebler, and R. E. Waltz, *Phys. Plasmas* **15**, 055908 (2008), APS07 issue.